AIAA JOURNAL
Vol. 47, No. 8, August 2009

Reference-Free Damage Detection Using Instantaneous Baseline Measurements

Steven R. Anton* and Daniel J. Inman†
Virginia Polytechnic Institute and State University, Blacksburg, Virginia 24061
and
Gyuhae Park‡
Los Alamos National Laboratory, Los Alamos, New Mexico 87545

DOI: 10.2514/1.43252

A novel method of guided wave-based structural health monitoring is developed in which no direct baseline data are required to identify structural damage. Conventional wave propagation structural health monitoring techniques involve the comparison of structural response data to a prerecorded baseline or reference measurement taken while the structure is in pristine condition. The need to compare new data to a prerecorded baseline can present several complications, including data management issues and difficulty in accommodating the effects of varying environmental and operational conditions on the data. To address the complications associated with baseline comparison, this new method accomplishes reference-free damage detection by acquiring what is referred to as an instantaneous baseline measurement for analysis. The instantaneous baseline technique is validated through both analytical and experimental testing. Analytical tests show that the instantaneous baseline method is able to correctly identify simulated damage. It is found experimentally that nonpermanent damage in the form of removable putty as well as permanent damage in the form of corrosion and cuts are all identifiable in thin aluminum plate test structures without direct comparison to baseline data when implementing the instantaneous baseline method.

Nomenclature

A_0, A_1	=	antisymmetric Lamb wave modes
a	=	peak cross-correlation value
b	=	sum of original modified cross-correlation values with damaged path subtracted
c	=	sum of scaled modified cross-correlation values
d	=	damaged path index
i	=	reference path index, also column index
j	=	comparison path index, also column index
k	=	row index
MCC_n	=	modified cross-correlation value after damaged path removal
MCC_s	=	scaled modified cross-correlation value
n	=	total number of paths, also number of samples in each Lamb wave signal
p	=	power of individual Lamb wave signals
p_m	=	mean power of all Lamb wave signals
r	=	principal component analysis ratio
S_0, S_1	=	symmetric Lamb wave modes
$\mathbf{V}$	=	matrix of eigenvectors of covariance matrix
V	=	voltage
v	=	eigenvector entry
$\bar{\mathbf{v}}$	=	mean of eigenvector entries
$\mathbf{X}$	=	matrix of Lamb wave data
x	=	entries in matrix of Lamb wave data
$\mathbf{\Lambda}$	=	diagonal matrix of eigenvalues of covariance matrix
λ	=	eigenvalue
$\mathbf{\Sigma}$	=	covariance matrix

Received 15 January 2009; revision received 24 March 2009; accepted for publication 31 March 2009.

*Ph.D. Candidate, Department of Mechanical Engineering, Center for Intelligent Materials Systems and Structures, 310 Durham Hall.

†G.R. Goodson Professor and Director, Department of Mechanical Engineering, Center for Intelligent Materials Systems and Structures, 310 Durham Hall. Fellow AIAA.

‡Engineering Institute.

I. Introduction

STRUCTURAL health monitoring (SHM) has gained a significant amount of attention in the research and industrial communities over the last two decades. The concept of actively monitoring structures for damage is of interest because it presents the ability to detect and locate damage in a structure before it can propagate and cause serious failure. The ability to know when and where damage has occurred in a structure can reduce the costs associated with scheduled inspections and the repair of failed structures, and also improve the overall safety of the structure.

Several successful guided wave-based SHM techniques have been developed in the literature. Review articles summarizing the relevant work on wave propagation-based SHM are presented by Giurgiutiu and Cuc [1], and Raghavan and Cesnik [2]. More specifically, methods have been explored for detecting damage in a variety of structures including thin metal plates [3–5], aircraft panels [6–8], composite materials [9–11], and civil structures [12–15]. These methods rely on some knowledge of the structure in a healthy state to identify damage. Typically, baseline measurements are recorded when a structure is pristine and are stored for comparison to future data for damage detection. Changes in the newly recorded data when compared to the baseline are used to identify structural damage. One concern with the use of these baseline subtraction methods is the ability to discern structural changes from the effects of varying environmental and operational conditions when analyzing the structural response of a system. Changes in environmental and operational conditions such as fluctuations in temperature, variation in surface moisture, and varying loading conditions can all cause the response of a structure to change significantly from the baseline measurement. The use of a standard baseline comparison method may falsely indicate damage or allow damage to go undetected in the presence of these varying conditions. Additionally, standard baseline comparison methods are unable to detect damage that exists in a structure before the installation of the health monitoring system, therefore, they are only useful for detecting future damage.

Several researchers have investigated the development of SHM techniques that take into consideration the effects of varying environmental conditions, specifically temperature changes. Sohn et al. [16,17] present works in which neural networks are trained using features extracted from healthy baseline data and from data taken under various environmental conditions. The network is trained to be

immune to environmental changes and only indicate damage when changes in the data do not correlate to the learned effects of varying environmental conditions. In a study presented by Lu and Michaels [18], a guided wave SHM technique is developed in which an extensive database of baseline measurements over a range of temperatures are first recorded for a structure. When new measurements are recorded, they are compared to each baseline and the closest match is used under the assumption that both measurements are recorded under nearly the same ambient temperature. In a similar method, works performed by Konstantinidis et al. [19] and Croxford et al. [20] both use a so-called optimal baseline subtraction to eliminate the effects of temperature change on structural measurements.

The major drawback to the aforementioned methods for temperature compensation in guided wave structural health monitoring is that a large amount of baseline data recorded under varying environmental conditions are required to detect damage from data recorded at an unknown temperature. It is not always possible to subject a real structure to all of the possible environmental conditions that it may encounter during the acquisition of a database of baseline measurements. Additionally, the management and storage of such a large database of measurements can present complications in the development of practical SHM systems.

In an effort to eliminate these complications, researchers have begun to develop wave propagation-based SHM techniques that do not rely on any prior baseline data. In the last few years, the creation of baseline-free structural health monitoring methods has been proposed in the research. Several studies have focused on time reversal acoustics as a method in which damage can be identified in a structure by essentially probing the structure for nonlinearities caused by damage [21–24]. Another method of baseline-free SHM uses the polarization characteristics of piezoelectric transducers and involves collocating transducers on both surfaces of a thin structure and exciting guided waves across different transducer pairs to identify damage [25].

The structural health monitoring method presented here is a novel and practical method of baseline-free SHM using simple algorithms and a relatively sparse network of transducers. This is accomplished through the use of instantaneous baseline measurements.

II. Instantaneous Baseline Methodology

The concept of instantaneous baseline structural health monitoring involves detecting damage without the use of prerecorded baseline data by acquiring an "instantaneous baseline" measurement each time a structure is interrogated. The structure is probed using a class of guided waves known as Lamb waves that propagate in thin plates and shells with free surfaces. Lamb waves are dispersive waves that travel in two distinct modes, known as symmetric and antisymmetric modes, in which displacements and stresses about the midplane of the host object are symmetric and antisymmetric, respectively. A comprehensive analysis of Lamb waves is given by Viktorov [26] and Rose [27]. The concept behind the instantaneous baseline measurement is that transducers can be placed on a structure such that pitch–catch Lamb wave propagation can be used to obtain common features of undamaged sensor–actuator paths that act as a baseline. The transducers must be placed such that the sensor–actuator paths are of equal length and that structural features and material properties are spatially uniform between transducers. In an isotropic structure, the initial Lamb wave arrival signals before any boundary reflections will be identical for different paths if the structure is undamaged. If damage is present along one of the paths, the Lamb wave signal recorded along that path will differ from the remaining signals. Features from the undamaged paths are used to create a statistical baseline allowing the separation of damaged paths without prior knowledge of the structure by monitoring changes in the Lamb wave shape, magnitude, and frequency. Figure 1 illustrates the concept of instantaneous baseline SHM where signals from undamaged paths are used to create an instantaneous baseline from which signals from damaged paths can be compared and signal differences are used to indicate damage. In structures that contain

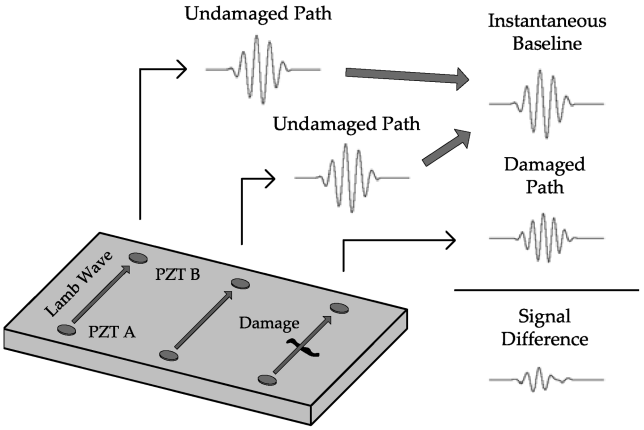

Fig. 1 Instantaneous baseline concept.

complex geometrical features such as ribs and rivets, careful sensor placement is required such that the structural features remain symmetric between comparison paths. In a case where a structure contains a rib, for example, transducer pairs creating a wave path across the rib may only be compared to other paths that similarly cross over the rib, and a separate set of paths may be composed of pairs located away from the rib.

The damage detection principle involved with the instantaneous baseline method is similar to that used in various nondestructive evaluation techniques including ultrasonic, infrared, and thermographic testing. The basic assumption involved with these defect detection techniques is that data can be collected over a large area of a structure, and the majority of those data will be recorded over undamaged sections, such that data recorded over damaged sections can be easily distinguished and identified. The instantaneous baseline method works under a similar principle in which the majority of the sensor–actuator paths are assumed to be recorded for undamaged paths, such that damaged paths can be easily identified when compared against the instantaneous baseline.

A. Piezoelectric Sensor Diagnostics

The instantaneous baseline method relies on the fact that Lamb wave signals recorded for two equally spaced paths will be identical if no damage is present in the vicinity of the paths. For this to hold true, not only must the material properties and geometric features be identical, but the electromechanical properties of the transducers exciting and receiving Lamb waves [most often lead zirconate titanate (PZT) piezoelectric devices] must also be identical. Slight differences in bonding condition or degradation of electrical/mechanical properties of PZT sensors can cause variation in the electromechanical coupling between transducers and the host structure, resulting in differences in Lamb wave signals from undamaged paths. A key component to any successful piezoelectric structural health monitoring system is the ability to assess the condition of the piezoelectric sensors and actuators installed on the structure being monitored. A technique referred to as piezoelectric active-sensor diagnostics is used in this study and presents the ability to evaluate both the bonding condition between a piezoelectric transducer and its host structure, as well as the mechanical and electrical properties of the device. The sensor diagnostics technique has been shown to successfully detect sensor/actuator faults by measuring the admittance of surface-bonded piezoelectric transducers at various frequencies and comparing plots of the imaginary part of the admittance versus frequency for each transducer. A detailed explanation of the sensor diagnostic technique and the mathematical derivations supporting it is presented by Park et al. [28–30]. The ability to diagnose the condition of PZT transducers is critical to the success of the instantaneous baseline method developed in this study, as the method relies on the fact that the shape, amplitude, and frequency of Lamb waves recorded for undamaged paths are the same and that an instantaneous baseline can be created from undamaged measurements.

B. Experimental Setup

A 4×4 ft (1.22×1.22 m), 0.0625 in. (1.5875 mm) thick 6061-T6 aluminum plate is selected as the test specimen used in this study. The test plates are of uniform thickness and assumed to be isotropic. The isotropy of the plates is confirmed during preliminary Lamb wave testing. Unlike typical aircraft structures, the test plates contain no complex geometric features such as ribs or stringers, however, the purpose of this study is to confirm the ability of the instantaneous baseline method to detect damage in simple, uniform structures. The health of three aluminum plates is monitored using two different piezoelectric transducer configurations. The first two aluminum plates are instrumented with an array of nine, 0.25 in. (6.35 mm) diameter, 0.01 in. (0.254 mm) thick circular piezoelectric devices surface bonded to the plates in a square grid pattern with 1 ft (0.30 m) between each patch. A third aluminum plate is instrumented with 13 PZT transducers fixed to the plate in a circular pattern with a radius of 18 in. (0.45 m). The deployment schemes along with the paths tested and total part coverage can be seen in Figs. 2 and 3. Two different configurations are chosen to determine what role the sensor pattern has in the ability of the instantaneous baseline technique to detect and potentially locate damage. The sensor placement is not optimized in either case. Optimal sensor placement is an important topic of research in the SHM community, as optimal sensor patterns may exist in which fewer sensors can be used to provide superior damage detection ability [31,32]. Pitch–catch Lamb wave propagation is used to perform instantaneous baseline structural health monitoring. Lamb waves are excited in a round-robin fashion such that each PZT transducer acts as both a sensor and an actuator. Three different path lengths are used in the square configuration and six path lengths are used in the circular configuration. A total of 28 paths are measured during each test for the square configuration and 72 paths are measured for the circular configuration.

Before testing, each aluminum plate is hung in a frame structure by running thin metal wire through small holes that are drilled in the upper corners of the plate. Once hung in the frame, the piezoelectric sensor diagnostics technique is used to assess the condition of the piezoelectric devices to ensure uniform performance. After measuring and recording impedance data for all transducers, the data are analyzed, any faulty sensors are replaced, and the process is repeated until all sensors are performing adequately. Upon ensuring uniform performance of all the PZT transducers, the plate can be inspected for damage. Lamb waves are excited in the plates and recorded at a sampling rate of 25 MHz. Each test requires a short amount of time, and so 50 averages are used to help eliminate noise in the recorded data before processing.

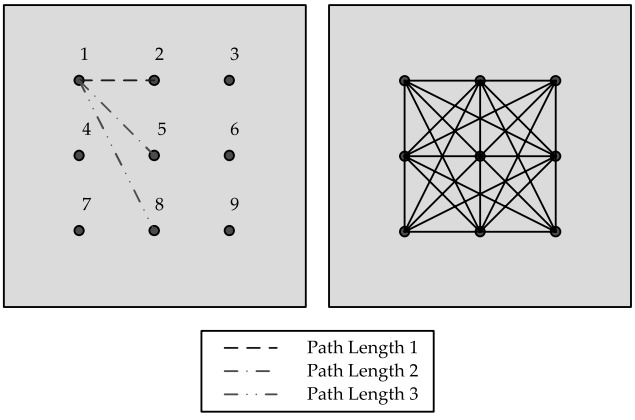

a) Path lengths **b) Overall part coverage**

Fig. 2 Square pattern path lengths and total part coverage.

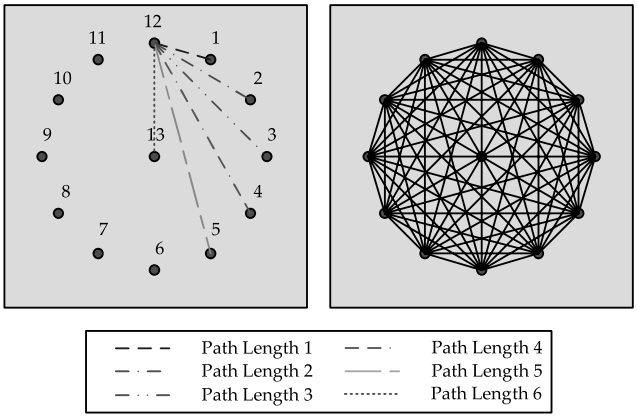

a) Path lengths **b) Overall part coverage**

Fig. 3 Circular pattern path lengths and total part coverage.

C. Excitation of Lamb Waves

The parameters of the excitation voltage signal must be chosen carefully to produce repeatable, single-frequency Lamb waves, exciting as few modes as possible with sufficient amplitude to propagate along the plate. A sinusoidal tone burst waveform, constructed by applying a Hanning window to a four-count sine wave, is selected as the excitation signal. A Hanning window is applied to excite the structure at a single frequency. An amplitude of 10 V peak-to-peak is chosen based on the limitations of the data acquisition hardware, however, an external amplifier is used to boost the signal to the PZT transducers to around 30 V peak-to-peak for adequate Lamb wave amplitude in the plate.

To help determine the best excitation frequencies to use, dispersion curves are generated for the test plates. Figure 4 shows dispersion curves calculated for 0.0625 in. (1.5875 mm) thick 6061-T6 aluminum with velocity plotted on the y axis and frequency plotted on the x axis. From Fig. 4, it can be seen that only the fundamental symmetric S_0 and antisymmetric A_0 modes exist up to a frequency of 1 MHz, therefore, the excitation frequencies are selected below 1 MHz to eliminate the excitation of higher-order

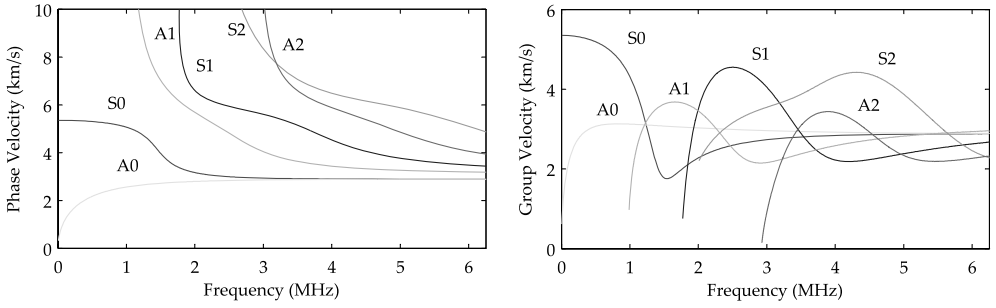

a) Phase velocity curve **b) Group velocity curve**

Fig. 4 Dispersion curves for 0.0625 in. (1.5875 mm) thick 6061-T6 aluminum.

modes. The selection of specific excitation frequencies for the experimental testing will be discussed later.

D. Damage Detection Algorithms

A key component of the instantaneous baseline structural health monitoring method is the use of damage detection algorithms that do not rely on previously recorded baseline data to analyze the condition of a structure. Three damage detection algorithms are developed that analyze various signal properties that are sensitive to different damage types in the plate test structures. Each damage detection technique is applied to the first A_0 mode wave arrival signal recorded along equal length paths, and each path length is analyzed separately. Only data from the first wave arrival are analyzed, therefore, symmetry in the boundaries of the test structure is not necessary as boundary reflection data are not used in the algorithms. Several analytical and experimental tests, described in the following sections, are performed on the aluminum tests plates and the results of these tests are used during the development of the algorithms.

All three damage detection algorithms are based on the fact that features from undamaged paths can be used to create an instantaneous baseline from which damaged paths can be separated. The algorithms create instantaneous baselines by assuming that the statistical majority of signals are from undamaged paths and have similar features. The statistical nature of the analysis techniques requires that there be a reasonably large ratio of undamaged to damaged paths. In the case where there are more damaged paths than undamaged paths, the algorithms will not be able to determine appropriate baseline features based on undamaged path characteristics. This should not present a problem in a structure that is constantly monitored where, at most, a few paths may become damaged at any one time.

1. *Cross-Correlation Algorithm*

The first damage detection technique developed involves the cross-correlation analysis of each signal compared with the remaining signals of other equal length paths. Cross-correlation analysis is used to determine the degree to which two signals are linearly related. To detect damage in the test structures, a modified cross-correlation value is calculated for each path and the values are used to indicate outlying or damaged paths. This technique first involves calculating the cross-correlation values of a single reference path compared to all the other paths, expressed mathematically by

$$\mathrm{MCC}\,(i) = \sum_{j=1}^{n} (1 - |a_i(j)|)^2 \tag{1}$$

where MCC is the modified cross-correlation value, n is the total number of paths, i represents the reference path index, j is the index of the comparison path, and a is the peak cross-correlation value for the specified path combination. A 500-point phase shift is integrated into the algorithm to account for small differences in sensor placement. The two input signals are shifted by 500 points and the cross-correlation value is calculated at each point along the shift. The variable a represents the peak cross-correlation value calculated during the shift. Considering the 25 Mhz sampling frequency, the 500-point phase-shift filters out only a small portion of the phase information such that phase distortion due to damage can still be detected. The correlation values are subtracted from one and squared so that outlying paths will have large modified cross-correlation values compared to statistically common paths. The process is repeated using each path as a reference path.

To produce a robust damage detection method capable of detecting multiple damaged paths, the cross-correlation data are further processed. Damaged paths are identified by investigating the effects of removing a potentially damaged path from the data set and recalculating the cross-correlation values. If a damaged path exists in the data set, the removal of the damaged path will cause the sum shown in Eq. (1) to decrease for every remaining path because the sum will no longer include the correlation value calculated when compared with the damaged path. Based on this fact, the cross-correlation algorithm calculates the percent difference between the sum of the original values of MCC when the damaged path is included in the calculations and the sum of the new values of MCC after the damaged path is removed from the data set. To calculate this percent difference, the path with the lowest correlation, that is, the greatest value of MCC, is first removed from the data set and the cross-correlation procedure is performed again on the remaining paths. The new modified cross-correlation values need to be scaled for comparison purposes to the original values because the new values represent the addition of only the remaining paths. The new values are scaled proportionally by

$$\mathrm{MCC}_s(i) = \mathrm{MCC}_n(i) + \frac{\mathrm{MCC}_n(i)}{n-1} \tag{2}$$

where MCC_n represents the new values of the modified cross-correlation value after a damaged path has been subtracted from the data set, and MCC_s is the scaled modified cross-correlation value. With the new, properly scaled, modified cross-correlation values calculated, the percent difference between the sum of the original values and the sum of the new values is calculated. The new scaled values can simply be summed, however, the original values contain one more entry than the new values, therefore, the modified cross-correlation value for the damaged path is subtracted from the sum of the original values. The summations are given by

$$b = \left(\sum_{i=1}^{n} \mathrm{MCC}_i\right) - \mathrm{MCC}(d) \tag{3}$$

$$c = \sum_{i=1}^{n-1} \mathrm{MCC}_s(i) \tag{4}$$

where b is the sum of the original values with the value of the damaged path subtracted, d represents the index of the damaged path, and c is the sum of the new values. The percent difference can finally be calculated by

$$\mathrm{PD} = \left(\frac{b-c}{b}\right) \times 100 \tag{5}$$

where PD is the calculated percent difference value. The percent difference is used to mathematically express how much the removed path affects the cross-correlation values of the remaining paths. If a damaged path is removed, the effect on the remaining paths will be significant. If an undamaged path is removed, the effect will be minimal. Using this concept, the path removal technique begins by removing the least correlated path and is repeated as many times as necessary to yield a relatively small percent difference value. Once an acceptable percent difference is reached, the algorithm stops and all the paths that were previously removed are designated as damaged.

Using this technique, it is necessary to set a threshold on the percent difference to detect damage, but not on the actual cross-correlation values calculated. As long as a typical percent difference for an undamaged structure can be estimated, this cross-correlation method can detect damage without the use of prerecorded baseline data. Typical percent differences of undamaged structures may vary considerably from structure to structure, therefore, it may be necessary to perform tests on structures that are known to be undamaged to estimate typical percent differences. Once these typical percent differences are found, however, this technique eliminates the need to record baseline data to detect damage.

2. *Power Spectral Density Algorithm*

The second damage detection technique developed involves calculating and analyzing the power spectral density (PSD) of each signal recorded. PSD is a measure of the amount of power in each frequency contained in a signal. The PSD is calculated using Welch's averaged modified periodogram method of spectral estimation using the first A_0 mode arrival of each signal. Once the PSD has been calculated for each of the equal length paths, the area under each

curve is determined, giving the average power of the signal over the entire frequency band. The mean value of the average power for all equal length paths is then found and compared to each individual path by calculating the following percent difference

$$\mathrm{PD}\,(i) = \left(\frac{p_m - p(i)}{p_m}\right) \times -100 \tag{6}$$

where PD is the percent difference value, i is the path index, p_m is the mean power of all paths, and p is the individual signal power. Using this percent difference calculation, paths containing a significantly different amount of energy from the mean can be isolated and declared as damaged. The percent difference is multiplied by -100 so that signals with a greater average power will show a positive percent difference and signals with a lower average power will show a negative percent difference.

The PSD method operates by first finding the percent difference for all paths. The path with the largest percent difference (either positive or negative) is selected and compared to a threshold value. As with the cross-correlation algorithm, the threshold value represents the typical percent difference found in an undamaged structure. If the path is above the threshold, it is declared damaged and is removed from the data set. The percent differences are recalculated excluding the damaged path and the process is repeated until the values lie below the threshold. All paths with percent difference values above the threshold are declared damaged. Through this technique, any path with a significantly increased or decreased average power can be identified and labeled as damaged.

3. *Principal Component Analysis-Based Algorithm*

The final data processing technique developed is based on the concept of principal component analysis (PCA). PCA is a method of reducing the order of multidimensional data sets for analysis purposes by calculating the dominant modes present in a set of data such that nondominant modes can be eliminated, thus reducing the size of the data set. PCA can be used for damage detection by calculating and analyzing the dominant modes of Lamb wave signals. Changes in the dominant component of each signal are used to determine how well the signals are correlated. PCA is performed by first calculating a covariance matrix of the entire data set. Each entry of the covariance matrix is a mathematical representation of the strength of the relationship between two of the signals. For PCA-based damage detection, the Lamb wave signals are first shifted using the same 500-point shift used in the cross-correlation algorithm to determine the positions of highest correlation for all signals. The shifted signals are then assembled into a data matrix defined as $\mathbf{X}$, where each column is a variable and each row is an observation. The covariance matrix is then calculated for the data matrix $\mathbf{X}$. The covariance and the covariance matrix are described by

$$\mathrm{cov}\,(\mathbf{x}_1, \mathbf{x}_2) = \sum_{k=1}^{n} \frac{[x_1(k) - \bar{\mathbf{x}}_1][x_2(k) - \bar{\mathbf{x}}_2]}{n-1} \tag{7}$$

$$\Sigma_{ij} = \mathrm{cov}(\mathbf{x}_i, \mathbf{x}_j) \tag{8}$$

where cov is the covariance, $\mathbf{\Sigma}$ is the covariance matrix, x_1 and x_2 are entries in the first and second columns of data, i and j are column indices of $\mathbf{X}$, k is the row index of $\mathbf{X}$, $\bar{\mathbf{x}}_1$ and $\bar{\mathbf{x}}_2$ are the mean values of the first and second columns of data, and n is the number of samples in each column of data. The covariance matrix is computed for each data set by using the first A_0 mode arrival data from equal length paths to form the data matrix $\mathbf{X}$.

Once the covariance matrix is calculated, the principal components are found by performing an eigendecomposition of the covariance matrix such that

$$\mathbf{\Sigma} = \mathbf{V}\mathbf{\Lambda}\mathbf{V}^{-1} \tag{9}$$

where $\mathbf{V}$ is a matrix for which the columns are the eigenvectors of $\mathbf{\Sigma}$, and $\mathbf{\Lambda}$ is a diagonal matrix containing the corresponding eigenvalues. The covariance matrix is of dimension $n \times n$, therefore, there will be n number of eigenvectors and n number of eigenvalues. The eigenvectors represent the principal components needed to describe the data set and the eigenvalues represent the importance, or strength, of each principal component. The eigenvectors with the largest corresponding eigenvalues are the dominant modes in the signal. Whereas conventional PCA would continue by eliminating the nondominant modes, and then using only the dominant modes to reconstruct a lower order data set, this damage detection method continues by analyzing the eigenvalues and eigenvectors.

In an ideal undamaged case, in which all of the signals from equal length paths are nearly identical, only one orthogonal mode would be necessary to represent all of the signals. This means that the first eigenvalue would far outweigh all the other eigenvalues and the first eigenvector would describe the dominant mode. In a case where damaged paths exist, however, multiple modes may be necessary to describe the data and the first eigenvalue may not far outweigh the others. The PCA-based damage detection algorithm uses two separate criteria to detect damage. The first criteria is to calculate the ratio of the second eigenvalue to the first eigenvalue given by

$$r = \frac{\lambda_2}{\lambda_1} \tag{10}$$

where r is the calculated ratio, λ_2 is the second highest eigenvalue, and λ_1 is the highest eigenvalue. If this ratio is above some threshold, then it can be concluded that there are two or more orthogonal modes needed to represent the signals, thus all of the signals are not well correlated and a damaged path exists in the data set. To identify which path is damaged, the second eigenvector is analyzed. The index of the highest entry of the second eigenvector corresponds to the path for which the second orthogonal mode is required to represent its signal, hence it represents the path that does not correlate well with the others.

Damage in a real structure, however, may not be significant enough to cause more than one orthogonal mode to be required to represent the signals. In this case, the second criteria for damage detection is used. This criteria involves analyzing the entries of the first eigenvector, which signify how well the first orthogonal mode represents each path signal. Damaged paths are detected by performing the following percent difference calculation

$$\mathrm{PD}\,(i) = \left(\frac{\bar{\mathbf{v}}_1 - v_1(i)}{\bar{\mathbf{v}}_1}\right) \times 100 \tag{11}$$

where PD is the percent difference, i is the path index, $\bar{\mathbf{v}}_1$ is the average of the first eigenvector entries, and v_1 is an entry of the first eigenvector. This percent difference value describes the strength to which the first dominant mode describes each path as compared to all the other paths. In the case of attenuation, shape change, or frequency change in a damaged path, the entry in the first eigenvector for the damaged path will be significantly lower than the average, causing a positive percent difference. If damage causes a signal to be amplified, then the first eigenvector entry for the damaged path will be larger than the average, causing a negative percent difference.

The PCA damage detection method operates by calculating the percent difference shown in Eq. (11) for each signal in a set of data from equal length paths. The path with the highest percent difference is selected and compared to a threshold value. If the percent difference is above the threshold, then the path is declared damaged and removed from the data set. The percent differences are re-calculated and the process is repeated until the highest percent difference lies below the threshold value. This algorithm, like the cross-correlation and PSD methods, uses a threshold value placed on the percent difference to indicate damage.

4. *Overview of Algorithms*

The damage detection algorithms developed here work to detect damage from Lamb wave signals without direct comparison to baseline data. In all three algorithms, a percent difference is calculated for equal length paths and used to define damage. The percent differences are compared to threshold values that do not need

to be calculated using baseline data. A simple knowledge of the typical percent differences on a similar undamaged structure is needed. This knowledge could come from a new, pristine structure, or from a small section of an old structure known to be healthy. Establishing a threshold for damage detection is a challenging task in all structural health monitoring techniques. A statistical approach can be used with the instantaneous baseline method, as with conventional methods, to analyze the variation in typical data files to establish appropriate threshold values. The key is that, once the threshold is set, baseline data do not need to be used for comparison each time a test is run, and a database of baseline measurements is not needed. In a structure subjected to global environmental or operational variations, the instantaneous baseline method is able to detect damage because signals are not compared to data recorded under different conditions. All of the data used in the algorithms are recorded under the same conditions, unlike traditional baseline comparison methods. When large environmental or operational changes are present, however, a new threshold value may need to be set if the changes cause the percent difference calculations to vary significantly for the undamaged structure. Additionally, local changes, such as temperature gradients, present an important topic in SHM research, however, they are not addressed in this study.

The percent difference calculations used in the algorithms allow for individual paths to be labeled as damaged, thus providing the ability to detect the presence as well as the general location of damage based on the intersection of multiple damaged paths. A limitation of the instantaneous baseline method is that it relies on a large ratio of undamaged paths to damaged paths to identify outlying signals. If more damaged paths than undamaged paths exist in a structure, the algorithms will not be able to determine a set of statistical features of undamaged paths to use as an instantaneous baseline for comparison. In many real structures, however, damage is introduced slowly and will not affect a majority of the paths at once. In a structural health monitoring system where the structure is frequently monitored, there should not suddenly be a high ratio of damaged to undamaged paths. Additionally, the percent difference calculations are sensitive to both damage in the structure and also to large differences in the undamaged path signals. If the undamaged paths contain a high amount of variability, the percent difference calculations may be unable to identify damage, therefore, the importance of material property and geometric uniformity between paths is affirmed.

Each algorithm developed is sensitive to different features of Lamb wave signals. The cross-correlation algorithm determines the extent to which the signals are linearly related. This algorithm is sensitive to shape change and frequency change, but insensitive to amplitude changes, as two identical signals with different amplitudes will have a perfect correlation. The PSD method determines the amount of energy in each signal, therefore, it is sensitive to amplitude change, but less sensitive to changes in shape and frequency. The PCA algorithm determines the dominant modes required to describe a set of signals and the weight of each dominant mode on each path. The algorithm is sensitive to shape, frequency, and amplitude changes. It should be noted that all three algorithms are insensitive to time of arrival changes. Both the cross-correlation and PCA algorithms include phase shifting to eliminate differences in time of arrival. Very little signal energy lies in the tails of the Lamb wave signals, therefore, the PSD algorithm is not sensitive to time of arrival changes. This insensitivity allows for small differences in the physical placement of sensors on a grid to be ignored by the algorithms so that damage is not falsely identified because of inconsistent sensor placement.

III. Analytical Testing

To aid in the development of the three damage detection algorithms created in this paper and to ensure that they function properly, various analytical testing is first performed. Known input signals simulating undamaged and damaged paths are created and processed. Undamaged signals are simulated using a four-count sine wave with a Hanning window applied. Damaged signals are simulated by applying phase, amplitude, and frequency variations to the undamaged signal. The three signal variations analyzed are not meant to represent specific damage cases. Actual structural damage will likely result in a combination of several types of variation. Several tests are performed during the development of the algorithms, and the results of the fully developed algorithms are presented in this section.

Four analytical tests are performed in which undamaged, phase-shifted, amplitude-shifted, and frequency-shifted signals are simulated and processed. In each case, nine signals are created and assembled into a matrix of test data which is used as the input to each damage detection algorithm. In the undamaged case, all nine signals are identical, where in the three damaged cases, one of the signals is modified. Time histories of the data simulated for each of the four analytical tests are presented in Fig. 5. From the figure, it can be seen that path 3 is chosen as the simulated damaged path. Additionally, it should be noted that all of the undamaged signals are identical for each simulation, so that it appears as if only a single signal is present in the time histories.

After processing the simulated data, the appropriate percent differences are calculated for each damage detection algorithm. A summary of the results for the four analytical tests is presented in

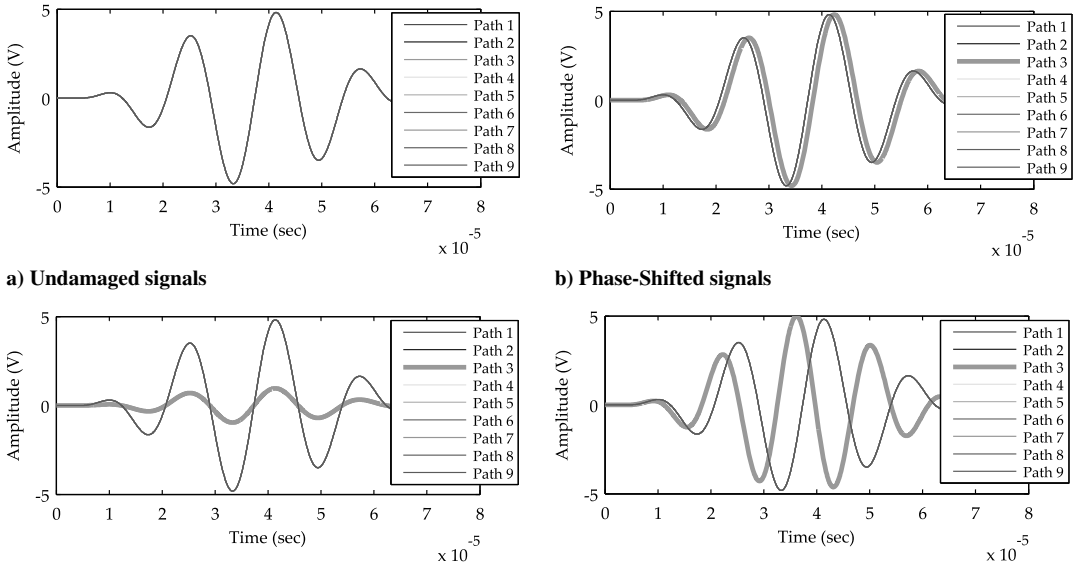

Fig. 5 Simulated damaged signal time histories.

Table 1 Analytical testing results

	Data analysis technique			
Analytical test	Cross correlation	PSD	PCA	PCA ratio, $\times 10^2$
Undamaged signals	0%	0%	0%	0
Phase-shifted signals	0%	0%	0%	0
Amplitude-shifted signals	0%	Path 3: −95.5%	Path 3: 78.0%	0
Frequency-shifted signals	Path 3: 100%	0%	Path 3: 14.2%	Path 3: 3.66

Table 1. First, nine identical signals are created to represent undamaged data. In response to the undamaged signals, the algorithms output percent differences of 0% and a PCA ratio of 0. These results are expected because all the signals are identical. The next test involves phase shifting one of the signals (path 3) by 25 points. Both the cross-correlation and PCA algorithms incorporate 500-point shifts, and the PSD method is insensitive to small phase shifts as it only compares the energy in the signals, therefore, it is expected that none of the algorithms will indicate damage. As shown in Table 1, the algorithms behave as predicted when analyzing the phase-shifted data, giving percent differences of 0% and a PCA ratio of 0. Next, the ability of each algorithm to detect a simulated damaged signal with attenuation is evaluated by decreasing the amplitude of one of the signals (path 3) by a factor of 5. The cross-correlation algorithm is insensitive to amplitude changes, and so it is expected that it will not indicate damage. The PSD and PCA algorithms, on the other hand, are sensitive to attenuation and amplification, therefore, it is expected that they will indicate path 3 as damaged. The results in Table 1 show that the algorithms again behave as predicted. The cross-correlation algorithm outputs a percent difference of 0%, whereas the PSD and PCA algorithms give percent differences of −95.5 and 78%, respectively. The PCA ratio is 0, which is expected because only one mode is required to describe the shape of all the signals as only the amplitude is altered. Lastly, the frequency of one of the signals (path 3) is shifted to determine the sensitivity of the algorithms to frequency changes. Both the cross-correlation and PCA algorithms are sensitive to frequency changes, whereas the PSD algorithm is not. The results in Table 1 show that the cross-correlation and PCA algorithms give percent differences of 100 and 14%, respectively, and the PCA ratio is 3.66×10^{-2}. In this case, the percent difference of 14% given by the PCA algorithm may or may not be large enough to declare the path as damaged depending on the threshold set, however, the cross-correlation and PCA ratio are large enough to indicate damage. The PSD algorithm, on the other hand, gives a percent difference of 0%. These results correlate well with the expected results.

Based on the results of the analytical testing, the damage detection algorithms behave as predicted. Given undamaged signals, the percent differences are calculated to be zero and no damaged paths are identified. Each algorithm is insensitive to signals with slight phase shifts which is necessary to eliminate false damage identification due to small sensor placement differences. Signals with amplitude and frequency shifts, however, are easily identified using a combination of all three damage detection techniques. Both the PSD and PCA algorithms are sensitive to amplitude changes, easily detecting path 3 as damaged in the test performed with amplitude-shifted signals. As expected, the cross-correlation algorithm is insensitive to amplitude changes. When a frequency-shifted signal is analyzed, the cross-correlation and PCA methods are both able to identify the damaged path. However, the cross-correlation method is much more sensitive to frequency shifts than the PCA algorithm. Overall, a combination of all three algorithms is able to easily identify signals with amplitude and frequency changes. The algorithms should also be able to identify shape change, which is similar to a combination of amplitude and frequency changes.

IV. Experimental Testing

With the ability of the damage detection methods to predict simulated damage verified, several experiments are performed on the aluminum test plates described previously. Experimental testing is first performed on undamaged plates to determine the path-to-path and test-to-test variability in Lamb wave measurements in the absence of damage. Next, putty is placed on the plates in various shapes and locations as a form of reversible simulated damage. The putty is used to establish the sensitivity of each algorithm in detecting damage and to help develop the algorithms. To determine the ability of the instantaneous baseline method to detect actual damage, several types of corrosion are induced in the plates. Additionally, a cut is slowly introduced at various depth levels in one of the plates. The results of the experimental testing are presented in the following sections.

A. Sensor Diagnostics

Before any Lamb wave data is recorded and analyzed on the test plates, the piezoelectric sensor diagnostics technique is performed on each plate to ensure consistent electromechanical coupling between the PZT transducers. For each plate, multiple installations of PZT transducers are carried out before uniform performance is achieved. An example of the sensor diagnostic measurements made on the first square pattern plate are given in Fig. 6. Measurements from the initial set of PZT transducers, shown in Fig. 6a, reveal a significant amount of variation in the admittance data, and the admittance of PZT 5 indicates that it is poorly bonded. After all nine PZT transducers are

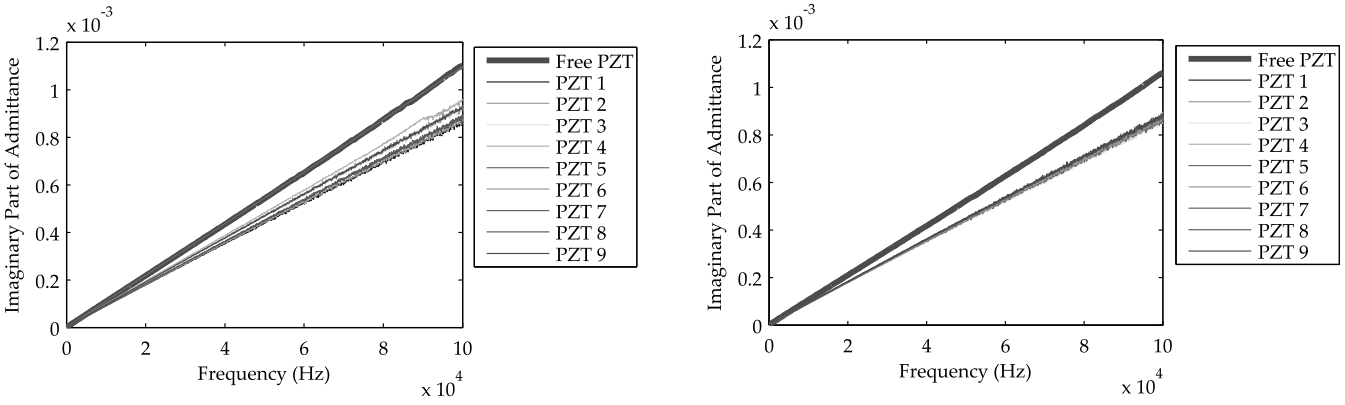

a) Initial set of PZT transducers **b) Final set of PZT transducers**

Fig. 6 Sensor diagnostic admittance measurements: first square pattern plate.

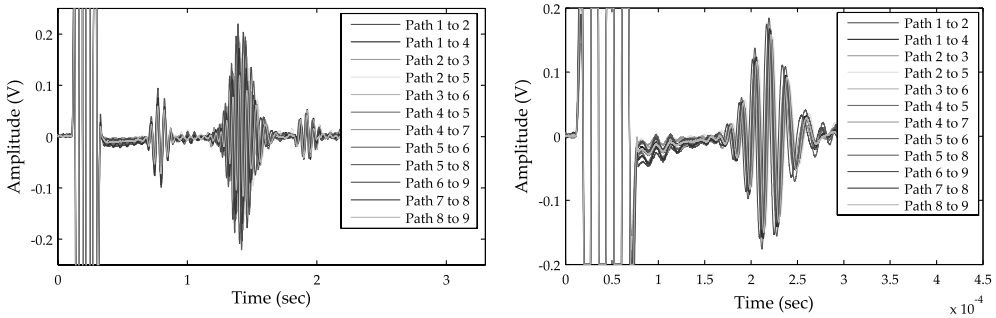

a) 180 kHz excitation frequency **b) 60 kHz excitation frequency**

Fig. 7 Lamb wave propagation data in square configuration test plate using 60 and 180 kHz excitation frequencies.

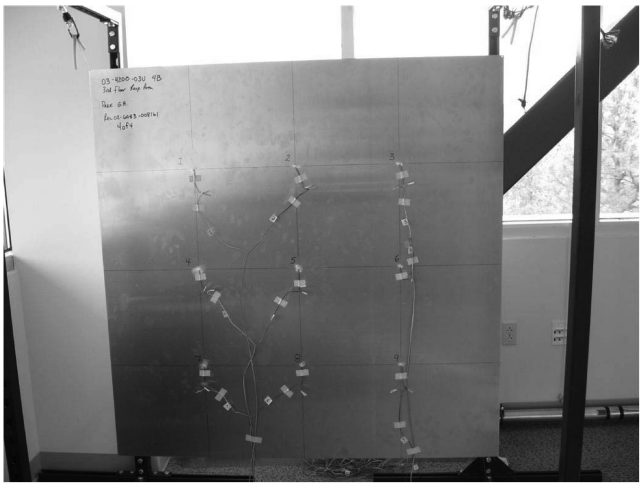

Fig. 8 Experimental setup with undamaged plate hanging in frame.

replaced, Fig. 6b shows the admittance data recorded for the final set of PZT transducers. The results show that the variation has decreased significantly, and no transducers appear to be poorly bonded or fractured.

B. Lamb Wave Excitation Frequency

Previously, it was established that an excitation frequency below 1 MHz would be selected to excite only the fundamental S_0 and A_0 modes. The optimal excitation frequency, however, will depend on the test configuration. Lamb waves are excited at frequencies from 40–200 kHz in each test plate to help determine the optimal frequency. It is found that there is a significant amount of path-to-path variation in signals at higher excitation frequencies. Additionally, it is also found that, at some lower frequencies, there is suppression of the S_0 mode. The phenomenon of exciting only a single mode at a particular frequency is known as Lamb wave tuning, and additional information on the topic is given by Santoni et al. [24]. Figure 7 shows Lamb wave time response data recorded in a square configuration test plate at both 60 and 180 kHz excitation frequencies to highlight these findings. Based on these observations, an excitation frequency of 60 kHz is used for the square pattern plates and 80 kHz is used in the circular configuration. The first A_0 mode arrival is used in the damage detection algorithms. A slightly higher frequency is used in the circular configuration to eliminate potential boundary reflections of any S_0 mode signal that may still exist when measuring data from the longest path length.

C. Undamaged Plates

The first few sets of data collected for each of the three aluminum plates are recorded with the plates in pristine condition. The isotropy of the plates is confirmed experimentally based on the low signal variations found in the undamaged cases (see Fig. 7b). A photograph of the experimental setup with an undamaged plate hung in a frame structure using thin metal wire is shown in Fig. 8. Data recorded from the undamaged plates is used to determine the typical signal variation of each path length. All of the undamaged data sets are analyzed using the cross-correlation, PSD, and PCA algorithms, and typical undamaged percent differences are established to set threshold values for damage detection. Average percent differences and typical PCA ratios from the undamaged square and circular configuration plates are shown in Tables 2–4. As discussed previously, actual undamaged baseline data do not have to be used when implementing the instantaneous baseline damage detection method on real structures. A simple knowledge of the percent differences of similar undamaged structures is needed to set the threshold.

D. Removable Putty Damage

Having obtained a knowledge of the Lamb wave response data and typical percent differences in undamaged plates, several tests are run in which damage is simulated using putty attached to the plates. The putty adds local mass and a boundary condition change that will alter the propagation of Lamb waves. Experiments are performed with a

Table 2 Typical percent differences for first square configuration plate

	Data analysis technique			
Path length	Cross correlation	PSD	PCA	PCA ratio, $\times 10^2$
1	20%	20%	10%	0.10
2	25%	15%	10%	0.10
3	30%	30%	20%	0.15

Table 3 Typical percent differences for second square configuration plate

	Data analysis technique			
Path length	Cross correlation	PSD	PCA	PCA ratio, $\times 10^2$
1	30%	25%	10%	0.05
2	60%	15%	10%	0.20
3	15%	35%	20%	0.35

Table 4 Typical percent differences for circular configuration plate

	Data analysis technique			
Path length	Cross correlation	PSD	PCA	PCA ratio, $\times 10^2$
1	15%	25%	15%	0.15
2	25%	40%	20%	0.20
3	20%	40%	20%	0.30
4	30%	40%	20%	0.50
5	15%	35%	20%	0.35
6	25%	45%	20%	0.45

variety of shapes and sizes of putty placed in different locations on each test plate to determine the sensitivity of each damage detection algorithm. Through the removable putty testing, it is found that percent difference increases of 10–20% above the normal undamaged values indicate paths of questionable condition, and increases above 20% are required to declare a path as damaged. Additionally, PCA ratio increases by 0.1×10^{-2}–0.2×10^{-2} indicate questionable paths, and increases above 0.2×10^{-2} indicate damaged paths. In practice, these thresholds can be adjusted to meet the needs of a particular application. Decreasing the thresholds will result in higher sensitivity to damage, but more chance for false damage identification, whereas increasing the thresholds will decrease sensitivity to damage, but lower the chance for false damage identification.

An example of the results of one of the removable putty tests in which a large piece of putty is placed between PZT 2 and 3 on the first square configuration plate is given in Fig. 9. The figure shows a photograph of the damaged plate as well as a plot of the time response data and the graphical output of each damage detection algorithm. From the time history, as well as the graphical outputs, path 2–3 can be easily identified as damaged. Each of the damage detection algorithms identifies path 2–3 as damaged with percent differences of 91.8, −90.9, and 70.4% for the cross-correlation, PSD, and PCA algorithms, respectively. These percent difference are all well above the thresholds. The PCA ratio is found to be 0.149×10^{-2}, which is less than the threshold for declaring damage, however, all three algorithms still declare path 2–3 as damaged.

E. Corrosion Damage

In the previous section, the instantaneous baseline method is shown to be able to detect removable putty damage. Next, permanent damage in the form of corrosion is induced on two of the test plates to better represent actual damage. Corrosion is a common cause of damage in mechanical, civil, and aerospace structures that can result in structural failure if undetected. Damage in the plates is induced through forced galvanic corrosion in which current is forced through a galvanic circuit containing an aluminum sacrificial anode. Five corrosion tests are performed including various locations and sizes of damage. Figure 10 shows photographs of each damage site as well as an illustration of the damage site locations and the paths successfully identified as damaged using each technique.

The first type of corrosion damage investigated is a small corrosion site measuring 1.04 in. (2.64 cm) in diameter placed in the middle of path 2–3 on the first square pattern plate, as shown in Fig. 10a. The corrosion is induced in nine discrete steps to determine the sensitivity of each damage detection algorithm to the depth of corrosion. From Fig. 10a, it can be seen that all three damage detection algorithms are able to identify path 2–3 as damaged, and the PCA method indicates two additional paths as damaged. Upon investigating the results from

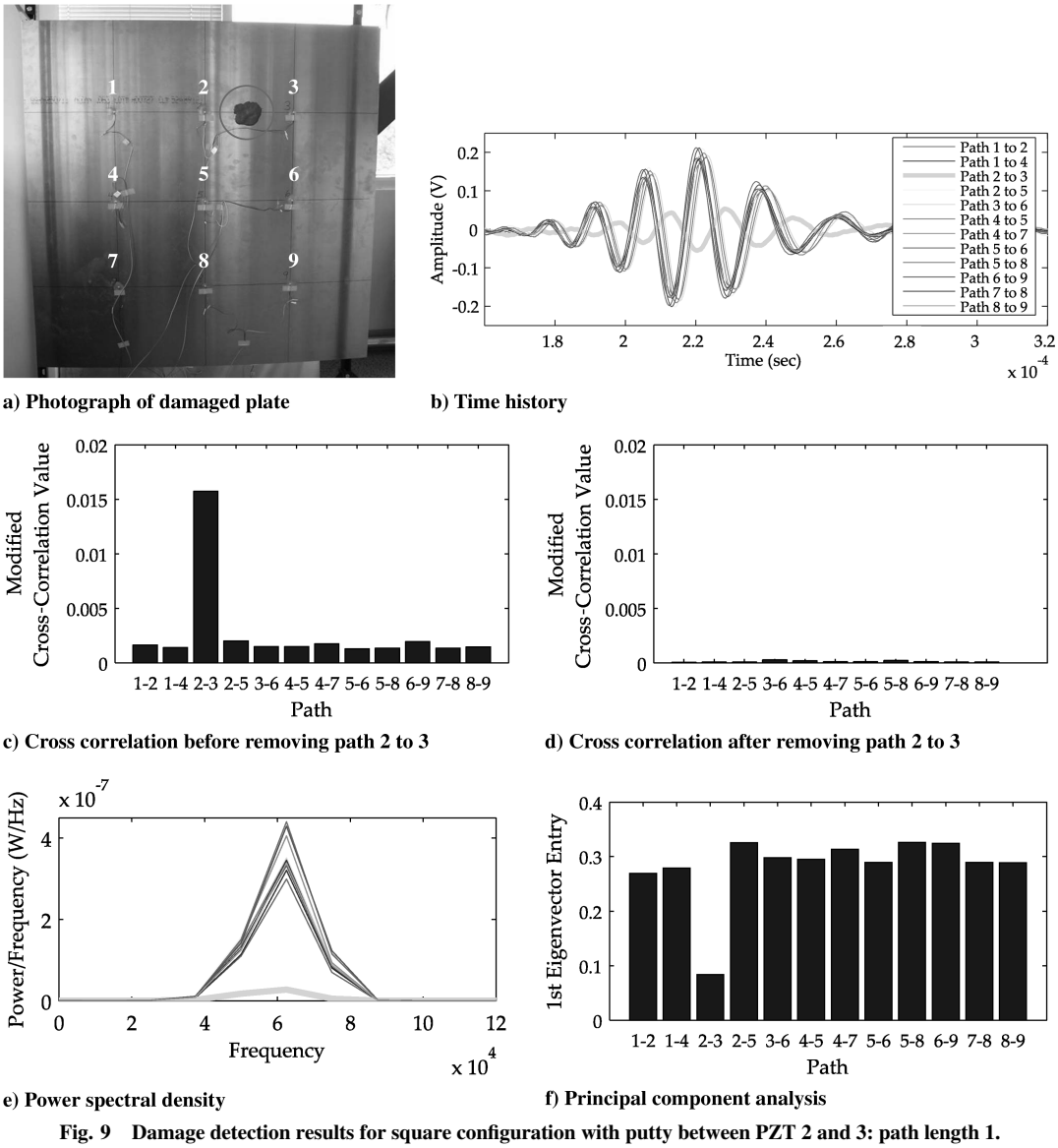

a) Photograph of damaged plate

b) Time history

c) Cross correlation before removing path 2 to 3

d) Cross correlation after removing path 2 to 3

e) Power spectral density

f) Principal component analysis

Fig. 9 Damage detection results for square configuration with putty between PZT 2 and 3: path length 1.

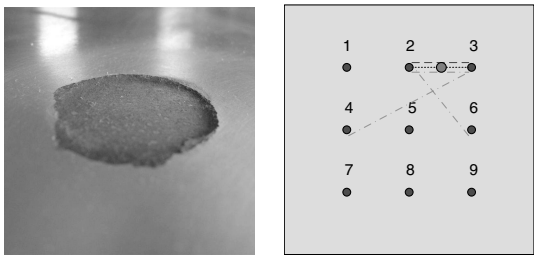

a) Small corrosion path 2-3 on first square plate

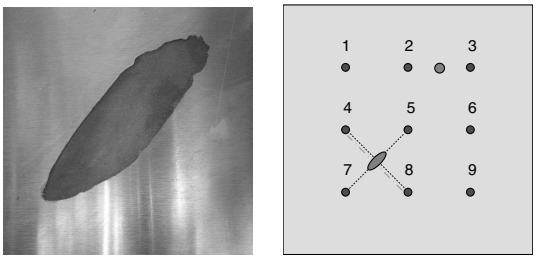

b) Elliptical corrosion path 5-7, 4-8 on first square plate

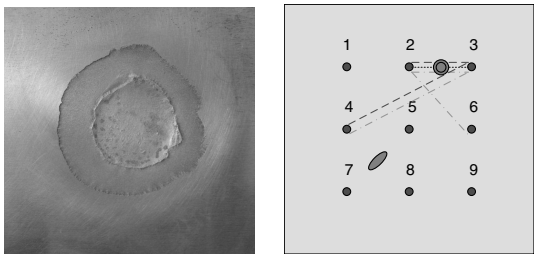

c) Concentric circle corrosion path 2-3 on first square plate

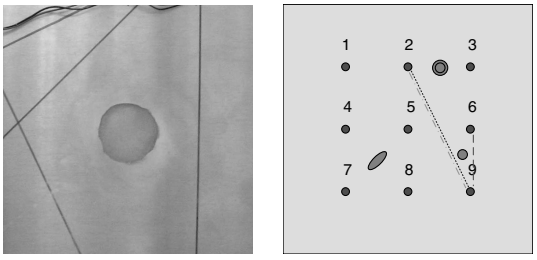

d) Off-path corrosion path 6-9 on first square plate

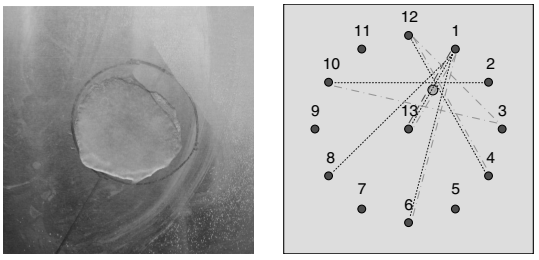

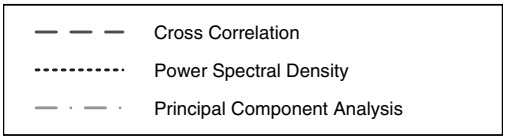

e) Small circle corrosion path 1-13 on circular plate

Fig. 10 Various damage tests identifying damaged paths for each damage detection algorithm.

path 2–3 as the depth of corrosion is increased, an interesting phenomenon is observed. It is found that, as the depth is increased, there is a critical depth at which the damage becomes difficult to detect using some of the algorithms. A summary of the results of all three damage detection algorithms highlighting this effect is given in Table 5.

From the results, it can be seen that, initially, the percent differences using the PSD and PCA techniques increase as the depth is increased. At the seventh and eighth depth levels, however, the percent differences decrease and then proceed to increase again at the final depth. This result suggests that there is some critical depth where damage cannot be detected using these techniques. Further investigation into the time histories over all of the depths reveals that, initially, the corrosion causes amplification of the Lamb wave response, followed by attenuation with further increases of the corrosion depth. The critical depth occurs when the amplitude of the damaged signal matches the amplitude of the undamaged signals. Although this result is unexpected, other research has also found amplification in signals due to corrosion [33]. It should be noted that the cross-correlation method does not detect path 2–3 to have the largest percent difference until the final two depth levels, and that a combination of all the damage detection techniques allow damage to be detected at all depth levels above 0.016 in. (0.406 mm). This final point shows the importance of combining all three damage detection methods to detect damage in real structures. Each algorithm is sensitive to different features and they have complimentary damage detection abilities.

The ability to detect noncircular corrosion damage is investigated next by inducing an elliptical corrosion site at the intersection of two of the paths on the first square configuration plate. The elliptical

Table 5 Percent differences in path 2–3 for variable corrosion damage

	Data analysis technique			
Depth, in./mm	Cross correlation	PSD	PCA	PCA ratio, $\times 10^2$
0.004/0.102	N/A	36.12%	−17.09%	0.079
0.007/0.178	N/A	39.30%	−18.51%	0.063
0.016/0.406	N/A	52.46%	−24.13%	0.069
0.016/0.406	N/A	62.21%	−28.16%	0.066
0.019/0.483	N/A	68.07%	−30.53%	0.090
0.021/0.533	N/A	71.66%	−32.01%	0.086
0.024/0.610	N/A	56.04%	−25.63%	0.110
0.029/0.737	54.22%	21.30%	−10.18%	0.175
0.033/0.838	98.48%	−80.06%	58.47%	0.361

corrosion site is placed at the intersection of path 4–8 and path 5–7, as shown in Fig. 10b, and has a length of 3.83 in. (9.73 cm), a width of 1.12 in. (2.85 cm), and a depth of 0.019 in. (0.483 mm). From the graphical results, it can be seen that only the PSD and PCA algorithms identify damage in the plate. Although this damage type proves more difficult to detect, several paths are still identified through a combination of the three algorithms.

The first two tests involve uniform corrosion sites, however, natural corrosion is often more irregular than the damage studied in the previous sections. To better simulate actual corrosion damage, a larger concentric circle of corrosion is next induced around the initial small corrosion site in path 2–3 on the first square configuration plate. Figure 10c shows a photograph of the concentric circle corrosion, which has a diameter of 1.84 in. (4.67 cm) and a depth of 0.018 in. (0.46 mm). The original corrosion site is sealed off, so that no further corrosion takes place there. Adding the concentric circle in the plate results in a slight decrease in the percent differences calculated for path length 1 for all three damage detection algorithms, however, damage is still identified using each technique. The addition of concentric circle corrosion does, however, result in additional paths from path lengths 2 and 3 showing damage, likely because of the increase in diameter of the corrosion. Overall, the damage detection methods are able to better identify the concentric corrosion as opposed to the original small circle of corrosion.

The final type of corrosion damage induced on the first square pattern plate is a small circular corrosion site located away from any of the direct signal paths on the plate to ensure that damage can be detected away from a direct path. The off-path circular corrosion site, shown in Fig. 10d, measures 1.24 in. (3.15 cm) in diameter, is 0.02 in. (0.51 mm) deep, and is located slightly off of path 6–9. Upon examining the results of the damage detection algorithms for the off-path corrosion site, three paths are identified to indicate the presence of the damage. The data recorded for the off-path corrosion damage is, however, affected by the fact that both the concentric and elliptical corrosion sites are present in the plate when recording Lamb wave data. The cross-correlation algorithm, for example, shows path 2–3 having the highest percent difference of 87.88% because of the concentric damage, however, path 6–9 does have the second highest percent difference at 59.41% once path 2–3 is removed from the data set. Although the sensitivity to the off-path damage is decreased because of the other damage sites present in the plate, the damage detection algorithms are still able to identify damage in the area near the corrosion site.

Although the majority of the corrosion testing is performed on the first square pattern plate, a corrosion site is also induced in the circular pattern plate to compare the effectiveness of both patterns to detect damage. A circular corrosion site in path 1–13 measuring 1.75 in. (4.45 cm) in diameter and 0.02 in. (0.51 mm) deep is induced in the plate, as shown in Fig. 10e. Analyzing the results of all three damage detection methods for the six path lengths in the circular configuration reveals that several paths are identified as damaged. The large amount of damaged paths identified indicates that the presence of corrosion damage, as well as the location of damage, can be determined using the instantaneous baseline method.

F. Cut Damage

The ability of the instantaneous baseline method to detect corrosion damage has been shown in the previous section, however, other forms of damage are present in mechanical structures. Often times, damage exists in the form of cracks in structural components. To simulate a crack, a small cut is slowly made in the second square pattern plate. The cut is placed between PZT 1 and 2, and seven discrete depth levels are tested, resulting in a final cut through the thickness of the plate measuring 0.04 in. (1.02 mm) wide and 0.8 in. (2.03 cm) long. Figure 11 shows photographs of the cut damage in the plate as well as the paths identified as damaged. The experimental results reveal that the damage is undetectable until the final cut when the plate is breached. The percent differences for the first six depths are just slightly above the normal undamaged percentages. When the cut is made through the plate, however, the cross-correlation method

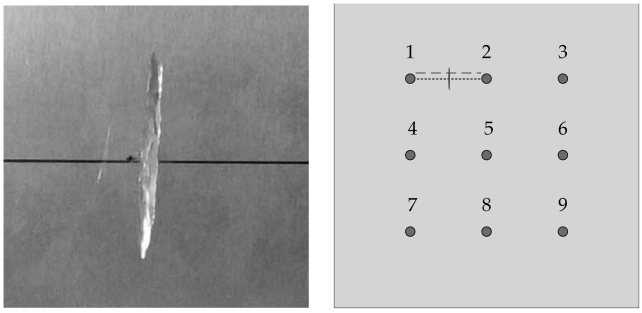

Fig. 11 Photographs of cut damage in path 1–2 on second square configuration plate.

yields a percent difference of 65.32% and the PSD algorithm gives a percent difference of 50.77% for path 1–2, thus identifying the path as damaged. The PCA algorithm indicates a percent difference of 29.78%, which is just under the threshold of 30% for declaring the path as damaged. These results suggest that the effects of a small cut that does not breach the plate are not great enough to indicate damage using the damage detection algorithms, however, a cut through the plate is detectable.

G. Summary of Experimental Testing

A variety of experimental tests are performed on three aluminum test plates in various damaged states. Tests are performed on undamaged plates and plates with removable putty, corrosion, and cut damage. Overall, the results of the experimental testing confirms the ability of the instantaneous baseline technique to detect damage without the use of prerecorded baseline data.

Results from the various corrosion testing performed suggest that a trend exists when increasing the depth of corrosion in the plate. Initially, corrosion causes amplification of Lamb wave signals, however, as the depth increases, the signals begin to attenuate. At some critical depth, the amplitude of damaged signals matches the amplitude of undamaged signals and the damage detection algorithms are unable to identify the damage. Further increases of the corrosion depth, however, result in more attenuation to the Lamb wave signals and damage can again be detected. This effect has caused certain depths of corrosion to be difficult to detect in the experimental testing.

Analyzing results from the cut damage testing reveals the fact that small cracks that are not through the thickness of the plate are difficult to detect. Given an excitation frequency of 60 kHz, which has a corresponding phase velocity of around 2300 m/s, the Lamb waves used to detect damage in the square configuration plate have a wavelength around 3.83 cm. This wavelength is likely too large to detect the small crack before it breaches the plate, therefore, a higher excitation frequency will provide better results for detecting smaller damage. This is consistent with a general rule of thumb in wave-based damage detection where waves can only detect damage greater than half the wavelength in size. Additionally, certain Lamb wave modes are sensitive to different types of damage and the S_0 mode may be better suited for crack detection [34].

Comparing the results from the first square configuration plate to the circular configuration plate, the effects of transducer pattern on damage detection can be analyzed. Each corrosion damage site induced in the square pattern plate is detected using the three damage detection algorithms, however, a comparison of the damage paths identified from the square and circular configurations reveals that the circular pattern is more capable of determining the exact location of damage. The circular pattern yields much better total part coverage, therefore, more paths are identified as damaged. The drawback to the circular configuration is that more PZT transducers must be used and many more data must be collected and processed to perform damage detection. A good compromise between transducer density and part coverage should be made when implementing guided wave-based SHM systems.

The corrosion and cut damage investigated in this paper reveals that a combination of all three damage detection methods is critical for the success of the instantaneous baseline damage detection technique. Each algorithm is sensitive to different features of Lamb wave propagation measurements. In some cases, a single algorithm may be suitable for damage detection if the damage type and its effect on the Lamb wave signals is known before testing, however, no single technique is able to identify all of the damage induced in the test plates. A combination of all three algorithms yields detection of damage in each case investigated in this research.

V. Conclusions

A novel guided wave-based structural health monitoring technique in which no direct comparison to baseline data is needed to detect damage is developed in this paper. The instantaneous baseline method operates by placing transducers on a structure such that pitch–catch Lamb wave propagation can be used to obtain common features of undamaged sensor–actuator paths that act as a baseline measurement. The fundamentals of the instantaneous baseline technique are outlined. The use of sensor diagnostics, the instrumentation of piezoelectric sensors on a test structure, the excitation and recording of Lamb wave signals, and the operation of the three damage detection algorithms developed are all discussed in detail.

The ability of the instantaneous baseline method to detect damage is demonstrated through both analytical and experimental testing. Results of the analytical testing show that the method responds as expected to undamaged, phase-shifted, amplitude-shifted, and frequency-shifted signals. All of the simulated damaged cases are properly identified using the three damage detection algorithms. Through the various experimental testing performed, it is found that the instantaneous baseline technique responds reasonably well to most damaged cases. Removable putty damage is easily detected, and, in each case, corrosion damage is identified by at least three damaged paths. The cut damage, however, proves more difficult to identify, and is only detectable once the cut has breached the plate. This result could likely be improved by increasing the Lamb wave excitation frequency to yield a shorter wavelength closer to the scale of the cut.

The development of a baseline-free damage detection technique presents several advantages to the structural health monitoring field. Conventional SHM methods use baseline comparison techniques where a prerecorded baseline measurement must be used to detect damage in a structure. The instantaneous baseline method is a baseline-free technique and does not rely on prior measurements, therefore, it is expected that the method can reduce the potential of falsely identifying damage or letting damage go undetected in structures subjected to varying environmental and operational conditions. An additional benefit of the instantaneous baseline method over conventional baseline comparison methods is that it can detect preexisting damage in structures. When applied to structures that may already contain damage, baseline comparison methods are unable to detect existing flaws. The instantaneous baseline method, however, can detect damage in new and existing structures as the identification of damage only depends on information from current measurements. Further work is underway to extend the proposed instantaneous baseline concept to more complicated structures, as only uniform, isotropic structures have been investigated in the current study. Both anisotropic structures and isotropic structures containing complex geometry such as welds and joints will be investigated. Additionally, more advanced signal processing will be incorporated to improve the performance of the proposed method. Overall, the development of this baseline-free technique aims to achieve more robust damage detection in the structural health monitoring field.

References

[1] Giurgiutiu, V., and Cuc, A., "Embedded Non-Destructive Evaluation for Structural Health Monitoring, Damage Detection, and Failure Prevention," *Shock and Vibration Digest*, Vol. 37, No. 2, 2005, pp. 83–105. doi:10.1177/0583102405052561

[2] Raghavan, A., and Cesnik, C. E., "Review of Guided-Wave Structural Health Monitoring," *Shock and Vibration Digest*, Vol. 39, No. 2, 2007, pp. 91–114. doi:10.1177/0583102406075428

[3] Tua, P., Quek, S., and Wang, Q., "Detection of Cracks in Cylindrical Pipes and Plates Using Piezo-Actuated Lamb Waves," *Smart Materials and Structures*, Vol. 14, No. 6, 2005, pp. 1325–1342. doi:10.1088/0964-1726/14/6/025

[4] Rajagopalan, J., Balasubramaniam, K., and Krishnamurthy, C. V., "A Single Transmitter Multi-Receiver (STMR) PZT Array for Guided Ultrasonic Wave Based Structural Health Monitoring of Large Isotropic Plate Structures," *Smart Materials and Structures*, Vol. 15, No. 5, 2006, pp. 1190–1196. doi:10.1088/0964-1726/15/5/005

[5] Malinowski, P., Wandowski, T., Trendalova, I., and Ostachowicz, W., "A Phased Array-Based Method For Damage Detection And Localization In Thin Plates," *Structural Health Monitoring*, Vol. 8, No. 1, 2009, pp. 5–15. doi:10.1177/1475921708090569

[6] Giurgiutiu, V., Zagrai, A., and Jing Bao, J., "Piezoelectric Wafer Embedded Active Sensors for Aging Aircraft Structural Health Monitoring," *Structural Health Monitoring*, Vol. 1, No. 1, 2002, pp. 41–61. doi:10.1177/147592170200100104

[7] Monnier, T., "Lamb Waves-Based Impact Damage Monitoring of a Stiffened Aircraft Panel Using Piezo-Electric Transducers," *Journal of Intelligent Material Systems and Structures*, Vol. 17, No. 5, 2006, pp. 411–421. doi:10.1177/1045389X06058630

[8] Cuc, A., Giurgiutiu, V., Joshi, S., and Tidwell, Z., "Structural Health Monitoring with Piezoelectric Wafer Active Sensors for Space Applications," *AIAA Journal*, Vol. 45, No. 12, 2007, pp. 2838–2850. doi:10.2514/1.26141

[9] Kessler, S. S., Spearing, S. M., and Soutis, C., "Damage Detection in Composite Materials Using Lamb Wave Methods," *Smart Materials and Structures*, Vol. 11, No. 2, 2002, pp. 269–278. doi:10.1088/0964-1726/11/2/310

[10] Sohn, H., Park, G., Wait, J. R., Limback, N. P., and Farrar, C. R., "Wavelet-Based Active Sensing for Delamination Detection in Composite Structures," *Smart Materials and Structures*, Vol. 13, No. 1, 2004, pp. 153–160. doi:10.1088/0964-1726/13/1/017

[11] Sekhar, B. V. S., Balasubramaniam, K., and Krishnamurthy, C. V., "Structural Health Monitoring of Fiber-Reinforced Composite Plates for Low-Velocity Impact Damage Using Ultrasonic Lamb Wave Tomography," *Structural Health Monitoring*, Vol. 5, No. 3, 2006, pp. 243–253. doi:10.1177/1475921706067739

[12] Na, W.-B., Kundu, T., and Ehsani, M. R., "Lamb Waves for Detecting Delamination Between Steel Bars and Concrete," *Computer-Aided Civil and Infrastructure Engineering*, Vol. 18, No. 1, 2003, pp. 58–63. doi:10.1111/1467-8667.t01-1-00299

[13] Park, S., Yun, C.-B., Roh, Y., and Lee, J.-J., "PZT-Based Active Damage Detection Techniques for Steel Bridge Components," *Smart Materials and Structures*, Vol. 15, No. 4, 2006, pp. 957–966. doi:10.1088/0964-1726/15/4/009

[14] Wu, F., and Chang, F.-K., "Debond Detection Using Embedded Piezoelectric Elements in Reinforced Concrete Structures, Part I: Experiment," *Structural Health Monitoring*, Vol. 5, No. 1, 2006, pp. 5–15. doi:10.1177/1475921706057978

[15] Wu, F., and Chang, F.-K., "Debond Detection Using Embedded Piezoelectric Elements for Reinforced Concrete Structures, Part II: Analysis and Algorithm," *Structural Health Monitoring*, Vol. 5, No. 1, 2006, pp. 17–28. doi:10.1177/1475921706057979

[16] Sohn, H., Worden, K., and Farrar, C. R., "Novelty Detection Under Changing Environmental Conditions," *Proceedings of SPIE: The International Society for Optical Engineering, Smart Structures and Materials 2001: Smart Systems for Bridges, Structures, and Highways*, Vol. 4330, Society of Photo-Optical Instrumentation Engineers, Bellingham, WA, March 2001, pp. 108–118.

[17] Sohn, H., Worden, K., and Farrar, C. R., "Consideration of Environmental and Operational Variability for Damage Diagnosis," *Proceedings of SPIE: The International Society for Optical Engineering, Smart Structures and Materials 2002: Smart Systems for Bridges, Structures, and Highways*, Vol. 4696, Society of Photo-

Optical Instrumentation Engineers , Bellingham, WA, March 2002, pp. 100–111.

[18] Lu, Y., and Michaels, J. E., "A Methodology for Structural Health Monitoring with Diffuse Ultrasonic Waves in the Presence of Temperature Variations," *Ultrasonics*, Vol. 43, No. 9, 2005, pp. 717–731.
doi:10.1016/j.ultras.2005.05.001

[19] Konstantinidis, G., Drinkwater, B. W., and Wilcox, P. D., "The Temperature Stability of Guided Wave Structural Health Monitoring Systems," *Smart Materials and Structures*, Vol. 15, No. 4, 2006, pp. 967–976.
doi:10.1088/0964-1726/15/4/010

[20] Croxford, A. J., Wilcox, P. D., Konstantinidis, G., and Drinkwater, B. W., "Strategies for Overcoming the Effect of Temperature on Guided Wave Structural Health Monitoring," *Proceedings of SPIE: The International Society for Optical Engineering, Health Monitoring of Structural and Biological Systems 2007*, Vol. 6532, Society of Photo-Optical Instrumentation Engineers, Bellingham, WA, March 2007, p. 65321T.

[21] Sohn, H., and Park, H. W., "Can Damage Be Detected Without Any Baseline Data?," *Proceedings of SPIE: The International Society for Optical Engineering, Health Monitoring and Smart Nondestructive Evaluation of Structural and Biological Systems IV*, Vol. 5768, Society of Photo-Optical Instrumentation Engineers, Bellingham, WA, March 2005, pp. 418–429.

[22] Kim, S. D., In, C. W., Cronin, K. E., Sohn, H., and Harries, K., "Reference-Free NDT Technique for Debonding Detection in CFRP-Strengthened RC Structures," *Journal of Structural Engineering*, Vol. 133, No. 8, 2007, pp. 1080–1091.
doi:10.1061/(ASCE)0733-9445(2007)133:8(1080)

[23] Park, H. W., Sohn, H., Law, K. H., and Farrar, C. R., "Time Reversal Active Sensing for Health Monitoring of a Composite Plate," *Journal of Sound and Vibration*, Vol. 302, Nos. 1–2, 2007, pp. 50–66.
doi:10.1016/j.jsv.2006.10.044

[24] Santoni, G. B., Yu, L., Xu, B., and Giurgiutiu, V., "Lamb Wave-Mode Tuning of Piezoelectric Wafer Active Sensors for Structural Health Monitoring," *Journal of Vibration and Acoustics*, Vol. 129, No. 6, 2007, pp. 752–762.
doi:10.1115/1.2748469

[25] Kim, S. B., and Sohn, H., "Instantaneous Reference-Free Crack Detection Based on Polarization Characteristics of Piezoelectric Materials," *Smart Materials and Structures*, Vol. 16, No. 6, 2007, pp. 2375–2387.
doi:10.1088/0964-1726/16/6/042

[26] Viktorov, I. A., *Rayleigh and Lamb Waves: Physical Theory and Applications*, Plenum, New York, 1967.

[27] Rose, J. L., *Ultrasonic Waves in Solid Media*, Cambridge Univ. Press, Cambridge, England, U.K., 1999.

[28] Park, G., Farrar, C., Rutherford, A., and Robertson, A., "Piezoelectric Active Sensor Self-Diagnostics Using Electrical Admittance Measurements," *Journal of Vibration and Acoustics*, Vol. 128, No. 4, 2006, pp. 469–476.
doi:10.1115/1.2202157

[29] Park, G., Farrar, C., di Scalea, F., and Coccia, S., "Performance Assessment and Validation of Piezo-Electric Active-Sensors in Structural Health Monitoring," *Smart Materials and Structures*, Vol. 15, No. 6, 2006, pp. 1673–1683.
doi:10.1088/0964-1726/15/6/020

[30] Park, S., Park, G., Yun, C.-B., and Farrar, C. R., "Sensor Self-Diagnosis Using a Modified Impedance Model for Active Sensing-Based Structural Health Monitoring," *Structural Health Monitoring*, Vol. 8, No. 1, 2009, pp. 71–82.
doi:10.1177/1475921708094792

[31] Guo, H., Zhang, L., Zhang, L., and Zhou, J., "Optimal Placement of Sensors for Structural Health Monitoring Using Improved Genetic Algorithms," *Smart Materials and Structures*, Vol. 13, No. 3, 2004, pp. 528–534.
doi:10.1088/0964-1726/13/3/011

[32] Rao, A. R. M., and Anandakumar, G., "Optimal Placement of Sensors for Structural System Identification and Health Monitoring Using a Hybrid Swarm Intelligence Technique," *Smart Materials and Structures*, Vol. 16, No. 6, 2007, pp. 2658–2672.
doi:10.1088/0964-1726/16/6/071

[33] Thomas, D., Welter, J., and Giurgiutiu, V., "Corrosion Damage Detection with Piezoelectric Wafer Active Sensors," *Proceedings of SPIE: The International Society for Optical Engineering, Health Monitoring and Smart Nondestructive Evaluation of Structural and Biological Systems III*, Vol. 5394, Society of Photo-Optical Instrumentation Engineers , Bellingham, WA, March 2004, pp. 11–22.

[34] Rose, J., Pilarski, A., and Ditri, J., "An Approach to Guided Wave Mode Selection for Inspection of Laminated Plate," *Journal of Reinforced Plastics and Composites*, Vol. 12, No. 5, 1993, pp. 536–544.
doi:10.1177/073168449301200504

J. Wei
Associate Editor